On the multiscale tribological signatures of the tool helix angle in profile milling of woven flax fiber composites

Faissal Chegdani*, Sabeur Mezghani, Mohamed El Mansori

Arts et Métiers ParisTech, MSMP-EA7350, Rue Saint Dominique, BP 508, 51006 Châlons-en-Champagne Cedex, France

ABSTRACT

The present study is focused on tribological and multiscale analysis for the machined surfaces of bi-directional flax fibers reinforced polypropylene composites. This is to track the multiscale effect of the helix angle of the cutting tool, related to its kinematic, on the cutting mechanisms. The results show that the helix angle has significant effect on the tribological performances which affect the tribo-contact interaction between the flax fibers and the cutting edge. The fibers orientation in the woven reinforcement has significant effect on the surface quality. The multiscale analysis reveals the pertinent scales that activate the helix angle effect.

1. Introduction

Natural fiber reinforced plastic (NFRP) composites become an industrial reality thanks to several economical, ecological and mechanical advantages [1–3]. These factors have motivated scientific researchers to explore new optimization methods of NFRP manufacturing processes [4,5]. Thus, finishing operations of NFRP composites is becoming a necessity. However, the practical finishing setup is difficult and still based on empirical rules [6–8] because the inherent activated physical mechanisms are still not well understood. This is due, on the one hand, to the multiscale complex structure of natural fibers as a stack of cellulosic cell walls [9]. The crystallinity of the cellulosic microfibrils, the cell walls shape and also the growth and the extraction conditions generate a high variability in the natural fiber mechanical properties [1,10,11]. On the other hand, the particular reinforcement structure of natural fibers inside the composites has to be taken into account because the natural fibers are gathered in bundles of several elementary fibers within the NFRP structure [12]. Consequently, the cutting process will solicit four different phases; the polymer matrix, the natural elementary fibers, the fiber/matrix interface and the interfaces between the elementary fibers. Therefore, it is important to take into account the cutting scales of NFRP materials which can be divided into three principal characteristic scales [13]:

- Microscopic scales that refer to the contact interaction between the cutting tool and the elementary fiber,
- Mesoscopic scales that refer to the contact interaction between the cutting tool and the fiber bundle,
- Macroscopic scales that refer to the contact interaction between the cutting tool and the overall structure of NFRP material (i.e. fiber bundles, polymer matrix and interfaces).

Therefore, multiscale study of the machinability of three different NFRP composites has been conducted [14] to analyze the scale effect and to correlate it with the machining characteristics of NFRP. It was observed that the roughness level of the machined surfaces decreases linearly with an increase in the fiber stiffness. This proves that the fiber stiffness has a significant effect on the cutting contact stiffness and the shearing mechanism of the natural fibers. However, the fiber stiffness cannot be the only factor that controls this cutting contact stiffness. Thus, this study aims to explore the multiscale effect of the cutting tool geometry, especially the helix angle, on the tribo-contact interactions between the cutting tool and the NFRP material and, then, the machined surface quality. The cutting experiments have been realized on bidirectional woven flax fibers reinforced polypropylene resin. This type of composite material is industrially well known thanks to its equivalent mechanical properties in the two main directions (longitudinal and transversal) which improve the homogeneity of the product performances. Multiscale surface analysis by 2D continuous wavelet transform [15,16] has been realized to detect the relevant analysis scales that activate the tool helix angle effect.

* Corresponding author. Tel.: +33 326 69 91 59; fax: +33 326 96 91 97.
E-mail address: faissal.chegdani@ensam.eu (F. Chegdani).

2. Materials and methods

2.1. NFRP workpieces

NFRP samples (Fig. 1(a)) are supplied by "Composites Evolution – UK" and are composed of 40% *vt* of bidirectional flax (BDF) fibers and 60% *vt* of Polypropylene (PP) matrix (approximately 50% *wt* for each constituent). The flax fiber reinforcement is in the form of 4×4 plain weave of flax yarns (Fig. 1(b)). The flax yarn diameter is approximately 1 mm. Typical properties of the flax fiber and the BDF/PP consolidated sheets are presented in Table 1. The fibers that are in the feed direction are called weft fibers and the fibers that are perpendicular to the feed direction are called warp fibers as shown in Fig. 1(b).

2.2. Machining operations

Machining experiments were realized using profile milling process on instrumented DMU60 monoBLOCK® five axes CNC machine (Fig. 2(a)) by testing two cutting configurations which are the up-milling and the down-milling. The up-milling is when the cutting edge attacks the cut surface from the zero thickness. The down-milling is when the cutting edge attacks the cut surface from the maximum thickness. In addition, three monobloc carbide end mills with identical properties and different helix angles ($H=0°$, $H=20°$ and $H=40°$) were tested as shown in Fig. 2(b–d).

Experimental system was mounted on a Kistler dynamometer (type 9255B) in order to measure the tridimensional cutting forces (F_x, F_y and F_z) as shown in Fig. 2(a). Tests have been conducted on dry cutting contact conditions at different feed rates. All other cutting parameters were kept constant (see Table 2). In order to get reliable results, each test was repeated three times under identical conditions and with a new cutting tool at each time.

2.3. Experimental measurements

Microscopic observations of BDF/PP surface state were made by scanning electron microscope (SEM) (JSM – 5510LV) at low vacuum mode. Typical representative surface morphology as induced by milling of each experimental configuration was taken into account for the microscopic analysis. Milled surface defects were evaluated by optical microscope (Nikon SMZ – 10).

3D topographic surface variations were measured by a three dimensional orange light interferometer (WYKO 3300NT). The milled surface was sampled at 515×515 points with a sampling length of 3.88 μm. The stitching mode is used to evaluate a surface dimension of 2×2 mm^2.

2.4. Multiscale approach by 2D continuous wavelet transform

Multiscale surface analysis involves the decomposition of topographic surface profiles into different roughness scales. This decomposition uses continuous wavelet transform which can be considered as a multi-channel filter system. The surface topography components pass through a filter bank which is a set of the contracting wavelets. It can be interpreted as a mathematical microscope, where the resolutions are the basic functions obtained from a single wavelet or mother wavelet by dilation (or compression) and translation [15–17].

The 2D directional continuous wavelet transform of a 2D surface topography $f(\vec{x})$ is defined by:

$$W_{\psi}^{f}(a,b,\theta) = \frac{1}{a} \int_{-\infty}^{+\infty} \int_{-\infty}^{+\infty} f\left(\vec{x}\right) \psi^*_{a,\vec{b},\theta}\left(\vec{x}\right) d\vec{x} \tag{1}$$

With $\psi_{a,\vec{b},\theta}\left(\vec{x}\right) = \psi_{a,\vec{b}}\left(r_{-\theta}\left(\vec{x}\right)\right)$ where $\vec{x} = (x,y)$ and r_{θ} represent the rotation operator:

$$r_{\theta}(x,y) = (x \cos \theta + y \sin \theta - x \sin \theta + y \cos \theta) \tag{2}$$

"a" is the contraction coefficient, $\vec{b} = (b_x, b_y)$ the translation coefficient in the x and y directions.

In this study we use the " Morlet 2D" wavelet given by the following expression:

$$\psi(\vec{x}) = e^{i\vec{\omega} \, o \, \vec{x}} e^{-\frac{1}{2}\left|\vec{x}\right|^2} + corr \tag{3}$$

With "$corr$" is a correction coefficient to satisfy admissibility conditions.

The wavelets generated by dilation "a" and translation "$\vec{b}$", $\psi_{b,a}(\vec{x})$ are given by:

$$\psi_{a,b}(\vec{x}) = e^{i\vec{\omega} \, o \left(\frac{\vec{x} - \vec{b}}{a}\right)} e^{-\frac{1}{2}\left|\left(\frac{\vec{x} - \vec{b}}{a}\right)\right|^2} + corr \tag{4}$$

Each component altitude of the surface topography "f" at the scale "a" in the "(x,y)" point coordinate $f_a\left(\vec{x},\theta\right)$ can be thus obtained in each analysis direction "θ" by inverse wavelets transform.

In this study, the 3D surface topographies decomposition are performed in two specific directions respectively in parallel ($\theta = 0°$) and perpendicular ($\theta = 90°$) to the feed direction. Then, for

Table 1
Mechanical properties of BDF/PP composite and its constituents.

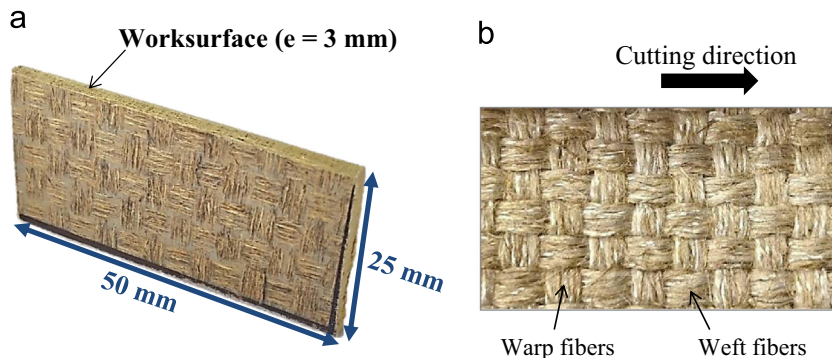|	Flax fiber	PP matrix	BDF/PP
Tensile modulus (GPa)	50	0.93	8.1
Tensile strength (MPa)	500	29.5	56
Maximum strain (%)	2	14	1.5

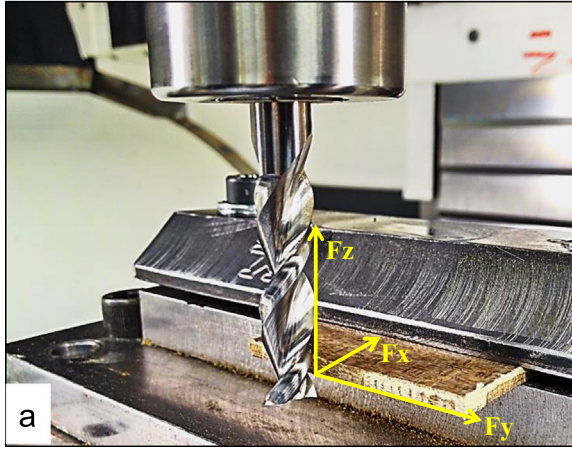**Fig. 1.** (a) BDF/PP workpiece. (b) Bidirectional flax fiber reinforcement.

Fig. 2. (a) Profile milling setup. (b) 0° helix angle end mill. (c) 20° helix angle end mill. (d) 40° helix angle end mill.
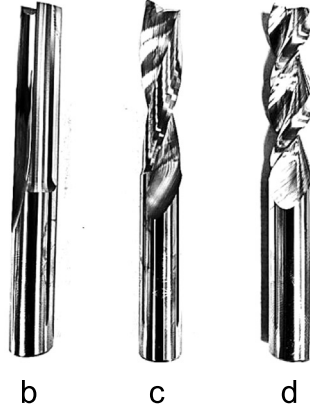
Table 2
Process parameters used for the profile milling tests.

Milling configuration	End mill helix angle (deg)	Feed (mm/ tooth)	Cutting speed (m/min)	Depth of cut (mm)
Up-milling Down-milling	0 20 40	0.08 0.12 0.16 0.2 0.24	100	1

each analysis direction, the arithmetic mean values are determined on the entire area of each surface scale component [15,16]. This allows to quantify the process effect over all the wavelength range from roughness to waviness, respectively in the tangential ($\theta = 0°$) and axial ($\theta = 90°$) direction. Two spectrums of arithmetic roughness amplitude are considered relative to the two analysis directions:

$$SMa_{//}(a) = \sum_{x=1}^{M} \sum_{y=1}^{N} \frac{\left| f_a\left(\vec{x}, 0\right)\right|}{MN} \tag{5}$$

$$SMa_{\perp}(a) = \sum_{x=1}^{M} \sum_{y=1}^{N} \frac{\left| f_a\left(\vec{x}, 90\right)\right|}{MN} \tag{6}$$

where "N" and "M" represent respectively the surface dimension in the x and the y directions.

3. Results and discussion

3.1. Microscopic surface quality

Fig. 3 shows the SEM images of the machined surface state that are divided into two zones which are the warp fiber zones (WPZ) and the weft fiber zones (WTZ). It can be seen that the WTZ generates high irregularities due to different fiber cutting behaviors. In fact, in the same WTZ, it can found some sheared fibers, some torn off fibers and some detached fibers that leave hollow zones on the milled surface. This is due to the tribo-contact between the cutting edge and each elementary fiber of the concerned weft fiber bundle. Indeed, depending on both the nature and the position of the contact between each elementary fiber and the cutting edge during its movement, the flax fiber can be sheared, torn off or detached from the milled surface according to its maintaining strength inside the composite as described in

Fig. 4. The fibers torn off and detachment are also due to the high flexibility of the natural fibers that are soft by nature due to their high cellulose content along the fiber axis and this characteristic gives them the ability to deform under fiber–tool interaction [18]. It is also due to the low compatibility between the natural fiber and the polymer matrix [19] which favors the fiber debonding.

For the WPZ, it can be seen that the zero helix angle allows having a better fiber shearing than that of 20° and 40° helix angles. The exceeded fibers extremities are more important in the case of non-zero helix angle. However, down-milling at 0° helix angle engenders important fibers debris on the milled surface while they are less obvious at the non-zero helix angles. This shows the important role of the tool helix angle for the chip clearance from the milled surface. Moreover, for the up-milling configuration, the fibers debris are not obvious at any helix angle value. Indeed, the exit of the cutting edge is apart from the milled surface in the up-milling configuration which allows a good chip clearance. On the other side, the exit of the cutting edge is on the milled surface for the down-milling configuration. Consequently, and without a helix angle for chip clearance, important fiber debris from the removed chip remains on the machined surface.

3.2. Tribological effects of helix angle

3.2.1. Cutting forces

Fig. 5 shows the tridimensional cutting forces (F_x, F_y, and F_z as shown in Fig. 2(a)) as a function of the tool feed for the three helix angle values. It can be seen that the cutting forces increase with an increase in the tool feed at all the cutting configurations. The effect of the cutting configuration is more obvious for the radial cutting forces (F_x) where the down-milling generates radial cutting forces higher than that of the up-milling configuration. However, the helix angle has an insignificant effect on F_x. Its effect is more relevant for the tangential cutting forces (F_y) which decrease significantly by helix angle increasing. Concerning the axial forces (F_z), they increase by helix angle increasing.

The resulting cutting force (F_R) in the (Y,Z) plan is initially oriented by a θ_0 angle at zero helix angle (Fig. 6(a)). This is due to the important vibrations induced by the contact interaction between the cutting edge and the composite material. Indeed, at zero helix angle, the contact entrance of the cutting edge into the material is brutal. There is no cutting continuity because there is not permanently a cutting tooth engaged in the workpiece. This causes a high variation in the cutting forces. At non-zero helix angle, the contact entrance of the cutting edge into the material is progressive (Fig. 6(b)). There is permanently a cutting tooth
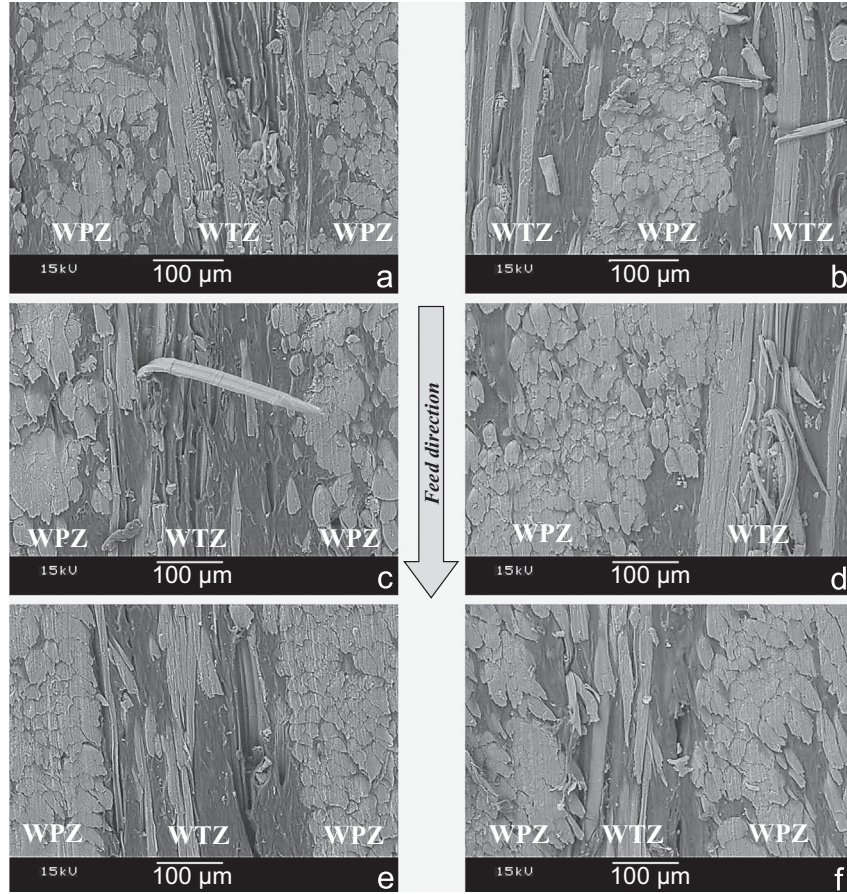
Fig. 3. SEM images of milled surfaces. Up-milling configuration with (a) 0° helix angle, (c) 20° helix angles and (e) 40° helix angle. Down-milling configuration with (b) 0° helix angle, (d) 20° helix angles and (f) 40° helix angle.
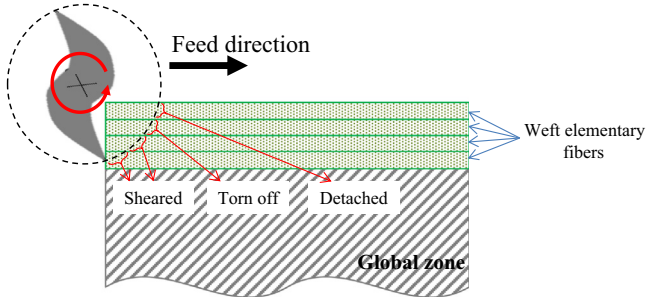

Fig. 4. Cutting mechanisms of weft elementary fibers regarding the cutting edge position.

engaged in the workpiece which generates cutting forces whose the values and the variations are less important.

By increasing the tool helix angle, F_R moves toward the Z direction as described in Fig. 6. This reorientation increases the Z component and decreases the Y component. It is important to note that the initial orientation angle for non-zero helix angle (θ' in Fig. 6(b)) is lower than that of zero helix angle (θ_0 in Fig. 6(a)) as the helix angle reduces the cutting vibrations.

According to the cutting forces analysis and the microscopic investigation of Section 3.1, it can be concluded that the brutal engagement of the cutting tool with zero helix angle stiffens the tribo-contact interaction between the cutting edge and the flax fibers which favors the fiber shearing during the milling process as it can be seen in the WPZ of Fig. 3(a) and (b). However, the progressive engagement of the cutting tools with non-zero helix angles decreases the tribo-contact stiffness between the cutting

edge and the flax fibers which favors the fiber deformation because of their transversal flexibility [13,14].

3.2.2. Frictional performances

For more understanding of the tribological phenomena during the milling process of BDF/PP composites, friction analysis has been conducted by calculating the apparent friction coefficient μ_{app} which is the ratio between the cutting force F_c and the radial force F_r in the tool coordinate system as shown in Fig. 7(a). F_c and F_r are calculated from the Cartesian cutting forces of Fig. 5 as described and explained in [20].

According to Fig. 7(b), down-milling configuration induces low friction comparing to the up-milling configuration. This is because the up-milling begins by rubbing the worksurface as the cutting edge attacks the cut surface from the zero thickness unlike the down-milling configuration (Section 2.2). The zero helix angle tool induces a very high friction coefficient during the milling operation. By increasing the helix angle, the friction coefficient decreases significantly while the effect of the tool feed is insignificant.

The apparent friction coefficient is a global concept. In the case of profile milling, it can be decomposed to three specific components:

$$\mu_{app} = \mu_{sh} + \mu_{df} + \mu_{ad} \tag{7}$$

where μ_{sh} is the shearing component, μ_{df} is the deformation component, μ_{ad} is the adhesion component. This decomposition can explain why the apparent friction coefficient is very high for the zero helix angle tool. Indeed, when milling with zero helix angle tool, there is increasing of the three components of μ_{app}. The
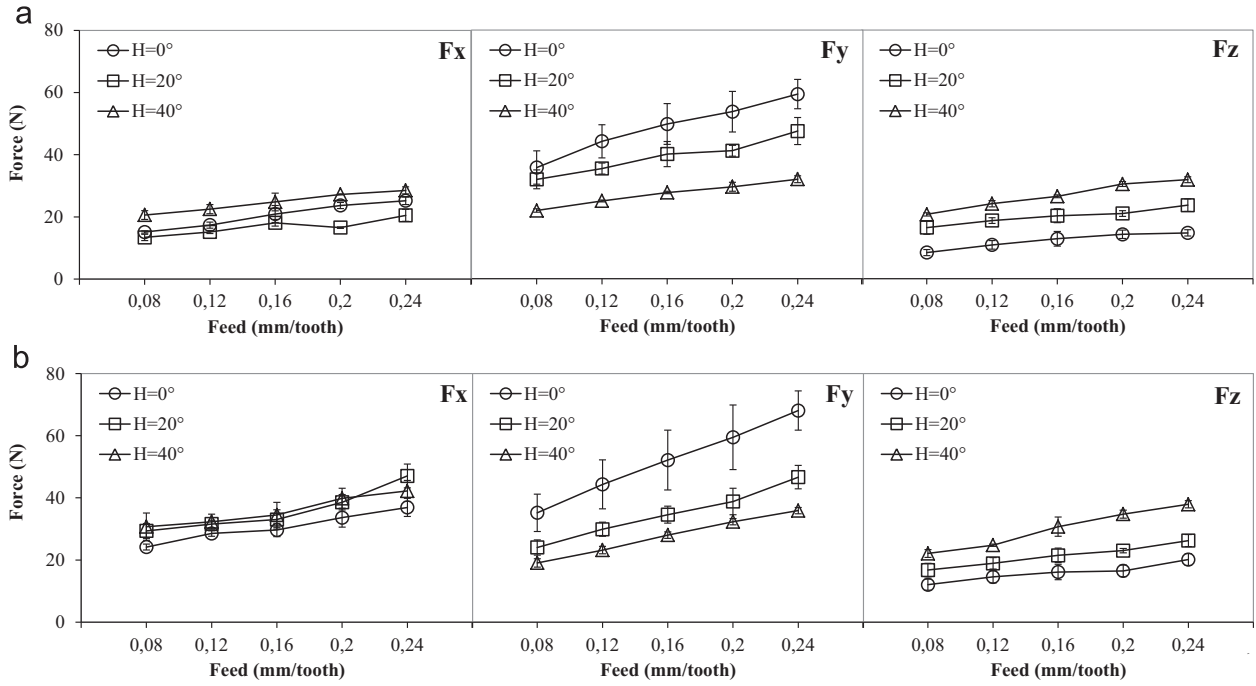
a

b

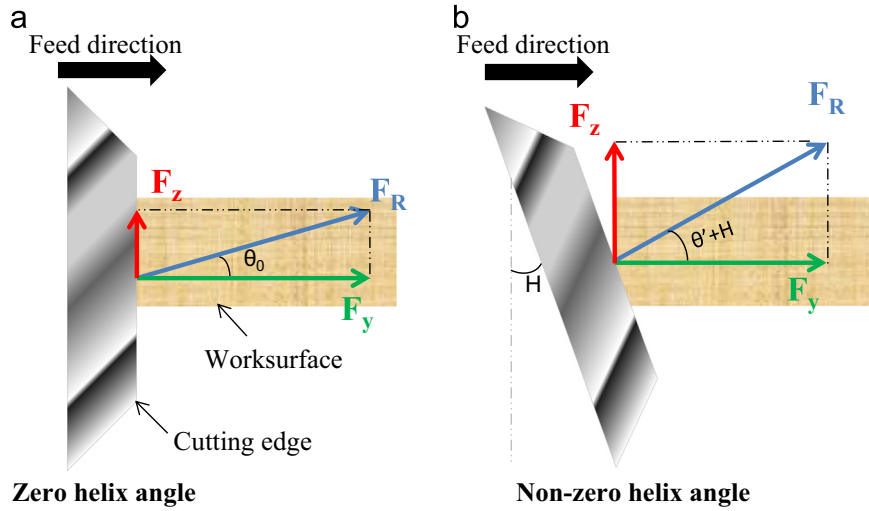**Fig. 5.** 3D tribological cutting forces for (a) up-milling configuration and (b) down-milling configuration.

a

b

Zero helix angle

Non-zero helix angle

Fig. 6. Schematization of the helix angle effect on the cutting force components in (Y,Z) plan.

a

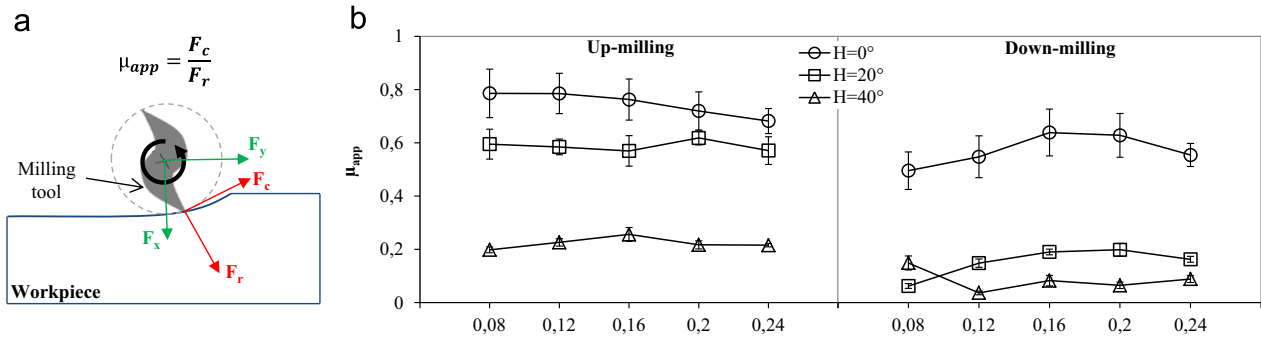$$\mu_{app} = \frac{F_c}{F_r}$$

b

Fig. 7. (a) Cutting forces in Cartesian and tool coordinate systems. (b) Apparent friction coefficient for all the cutting configurations.

rapid engagement of the zero helix angle cutting edge increases the shearing component (Section 3.2.1). The good fiber shearing with zero helix angle tool allows a large contact area between the tool flank face and the polymer matrix because of the absence of the uncut fiber extremities on the milled surface. It is well known that adhesion and deformation are important in the contact with
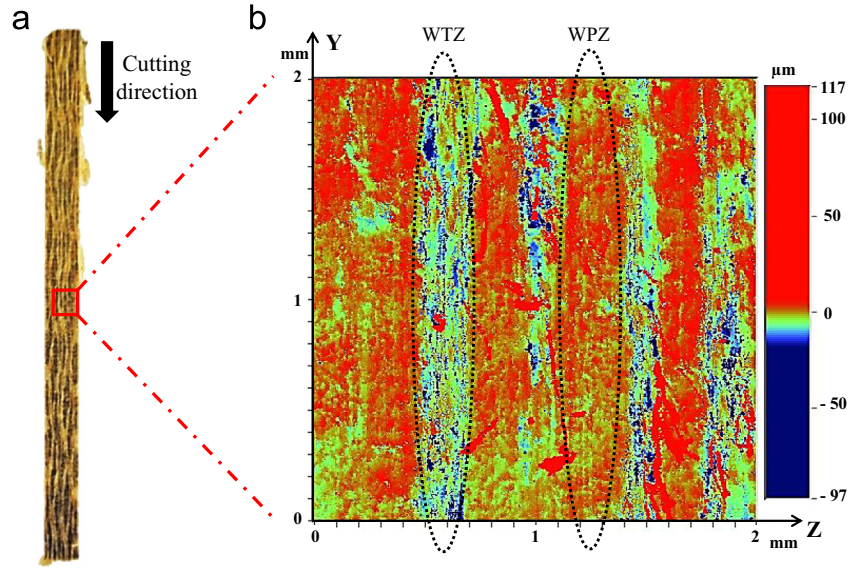
Fig. 8. (a) Full worksurface of BDF/PP after milling. (b) Interferometry image of the milled surface of BDF/PP.
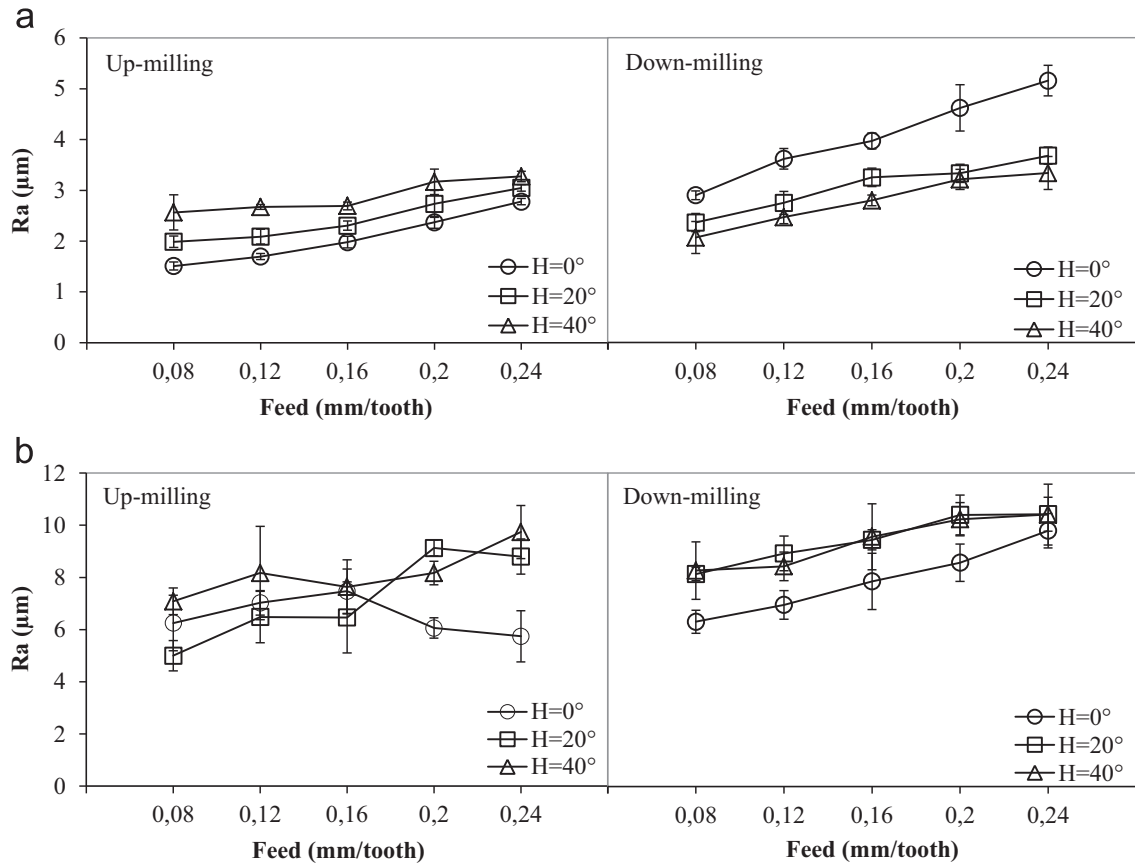

Fig. 9. Arithmetic mean roughness of the milled surfaces in the feed direction (a) at WPZ and (b) at WTZ.

polymer materials [21,22] and their components in the apparent friction coefficient will significantly increase by increasing the contact area between the polymer matrix and the cutting edge. On the other side, increasing the tool helix angle increases the uncut fiber extremities on the milled surface which will reduce the contact area between the flank surface and the polymer matrix. These uncut fiber extremities act as a third solid body lubricant by reducing the friction thanks to the non-abrasive character of the natural fibers as demonstrated by some tribological pin-on-disc studies [18,23,24]. Therefore, the three components of the apparent friction coefficient decrease by tool helix angle increasing. These induced tribological signatures lead to different cut surface modifications at various scales as discussed in the following section.
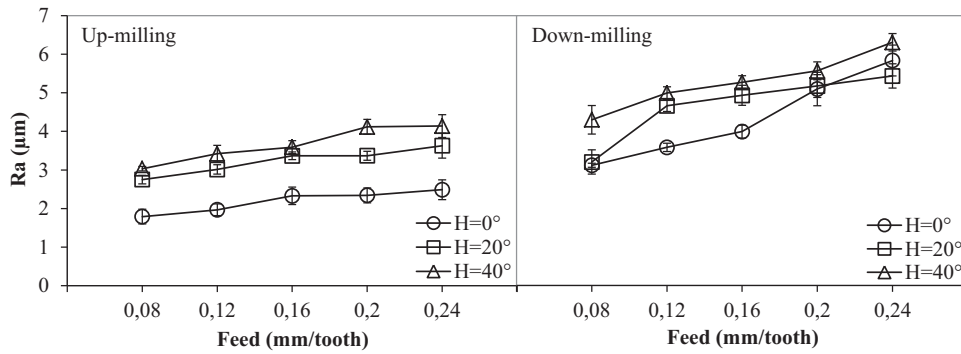
Fig. 10. Arithmetic mean roughness of the milled surfaces in the axial direction.

3.3. Surface roughness analysis

According to the interferometry image (Fig. 8) of the milled surface, there is a high difference in the surface variation amplitude between WTZ and WPZ. Thus, the smartest methodology for analyzing the surface roughness is to study the surface roughness in the feed direction (*Y* direction of Fig. 8) for the WTZ and WPZ separately. This will allow evaluating distinctly the contribution of the weft fibers and the warp fibers on the induced roughness of the milled surfaces.

Fig. 9 shows the mean arithmetic roughness (R_a) in the *Y* direction at the WPZ and the WTZ. Globally, the surface roughness increases by feed increasing. It shows that the surface roughness at the WTZ is much higher than that of WPZ with high standard deviation of R_a values in the WTZ which confirms the SEM observations of Section 3.1.

In the WPZ (Fig. 9(a)), increasing the helix angle of the cutting tool slightly increases the surface roughness for the up-milling configuration. However, the surface roughness for the down-milling configuration does not behave in the same way. In fact, there is not a significant difference between the surface roughness generated by the 20° helix angle and that generated by the 40° helix angle. Nevertheless, the 0° helix angle induces the highest surface roughness which increases significantly by feed increasing. This can be due to the important fibers debris that are observed in the SEM images (Fig. 3(b)) which can increase the irregularities amplitude of the measured surface topography at these zones.

In the WTZ (Fig. 9(b)), no difference detected between the tool helix angle effects for the up-milling configuration until the feed value of 0.16 mm/tooth. After this feed value, the surface roughness induced by the 0° helix angle become much lower than that of 20° and 40° helix angles which behave in the same way. For the down-milling configuration, the 0° helix angle generates the lowest surface roughness at all the feed range while no difference was observed between the roughness levels induced by 20° and 40° helix angles.

On the other hand, the R_a criterion had also been evaluated for the milled surfaces in the axial direction (*Z* direction of Fig. 8). The surfaces roughness in the *Z* direction is shown in Fig. 10 for both the up-milling and the down milling configurations. It shows that the surface roughness levels for the down-milling are higher than that of the up-milling for all the cutting configurations. The effect of the tool helix angle is more obvious at the up-milling configuration where the 0° helix angle induces the lowest surface roughness but the 20° and the 40° helix angles seems to behave in the same way.

It can be concluded that milling the BDF/PP composites by zero helix angle end mill at 0.08 mm/tooth of tool feed and using the up-milling configuration can provide an efficient fiber shearing during the machining operation (i.e. ductile cutting regime). This will hence reduce the milled surface roughness.

3.4. Multiscale surface roughness analysis

In Section 3.3, the effect of helix angle has been determined by separating the tangential direction from the axial direction and the warp fiber zones from the weft fiber zones. However, standard surface analysis is not able to discriminate the effect between 20° helix angle and 40° helix angle because they seem to behave in the same way. This can be due to the global scale inside which the surface roughness analysis is realized. Therefore, the multiscale surface analysis aims to reveal the pertinent analysis scales where the helix angle effect on the milled surface roughness is significantly activated.

Fig. 11 shows $SMa_\perp(a)$ and $SMa_{//}(a)$ parameters for the up-milling and the down-milling configurations in the axial (*Z*) and the tangential (*Y*) directions respectively. It can be seen that the roughness level is at its minimum for the microscopic scales and the multiscale surface roughness induced by both 20° and 40° helix angles seems to behave in the same way. It can be also observed that the roughness level increases by scale increasing. The helix angle effect starts to be obvious from the scale 50 μm which refers to the minimum of technical flax fiber diameter. The roughness level continues to increase until reaching its maximum at the scale 500 μm which refers to the maximum fiber bundle diameter. For the axial direction, 500 μm is the most relevant scale for discriminating the helix angle effect. For the tangential direction, the scales close to 500 μm (between 300 and 700 μm) are the most relevant of the irregularities of the roughness amplitude caused by the weft fiber zones as explained in Section 3.3.

According to the multiscale surface roughness analysis by the continuous wavelets transform, it can be concluded that the pertinent scales to study the helix angle effect are between 50 μm and 1 mm which refers to the technical fiber diameter and fiber yarn diameter, respectively. However, at the tangential direction, the high roughness variability caused by the weft fiber cutting arises at the scales between 300 and 700 μm.

3.5. Fluffing defects of milled surfaces

Fluffing defect is among the well-known surface damages in the composites. It takes place at the periphery composite layers that suffer from low fiber maintaining during the cutting interaction. This causes the break of the fiber–matrix interface and the fibers inside the periphery layers remain uncut. The fluffing defect is reflected by the top fluffing length, which refers to the uncut fibers length at the exit of the cutting edge (Δx of Fig. 12(a)), and the bottom fluffing length, which refers to the uncut fibers length at the entry of the cutting edge (Δy of Fig. 12(a)).
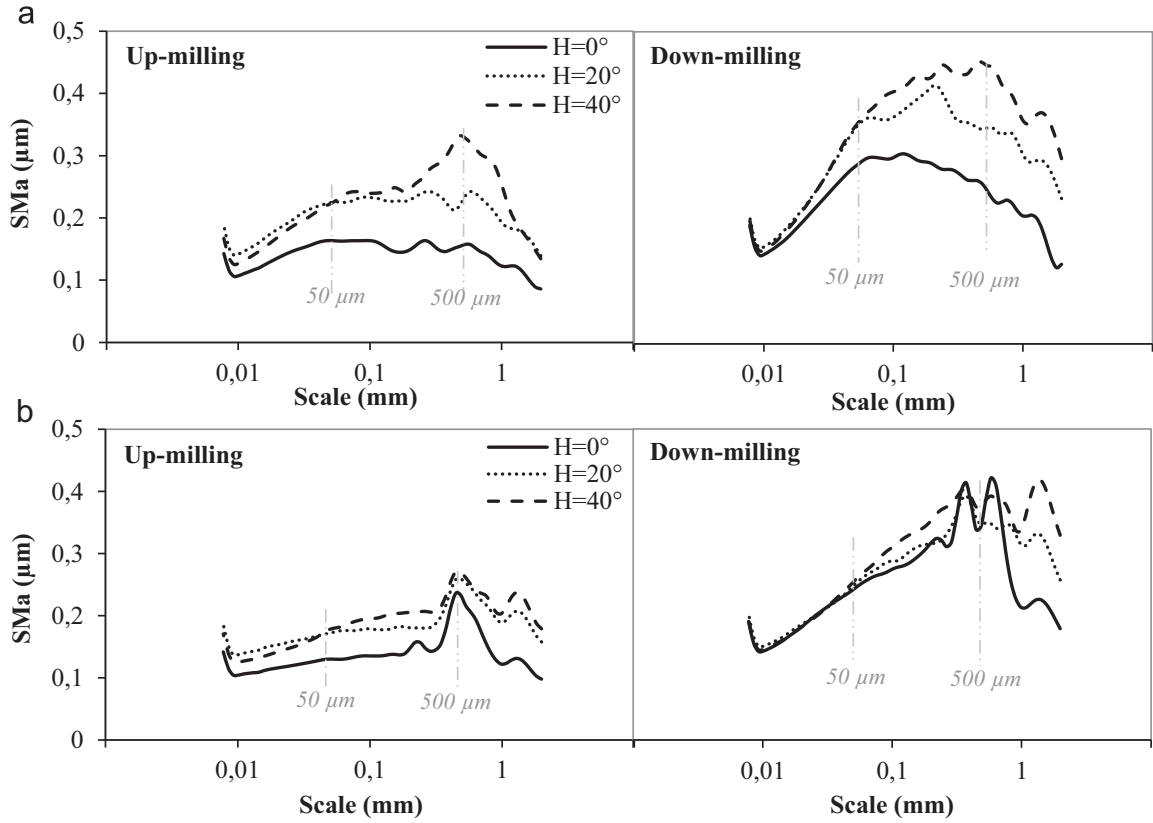
Fig. 11. Multiscale surface roughness spectrum of BDF/PP (a) in the axial direction and (b) in the tangential direction.
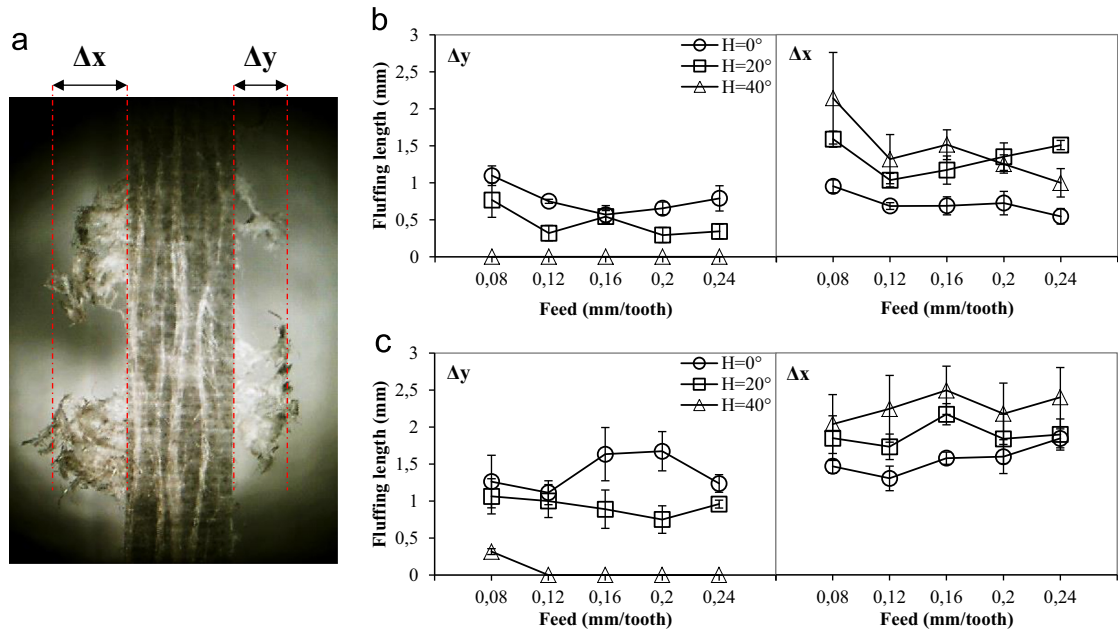

Fig. 12. (a) Optical microscope image of the worksurface showing the fluffing area. (b) Fluffing length for the up-milling configuration. (c) Fluffing length for the down-milling configuration.

The evaluation of fluffing defects in Fig. 12 shows an insignificant dependence of the tool feed. For both up-milling configuration (Fig. 12(b)) and down milling configuration (Fig. 12(c)), zero helix angle tool induces the same fluffing length at the top and the bottom of the work-surface. Increasing the helix angle increases the top fluffing and decreases the bottom fluffing until becoming zero for the 40° helix angle.

The relationship between the fluffing defect and the tool helix angle is essentially due to the contact interaction between the cutting edge and the flax fibers inside the periphery layers of the composite workpiece. Indeed, at the bottom periphery of the worksurface, the more the helix angle is high, the more the fibers inside the bottom periphery have a strong maintaining during the cutting operation thanks to the above stacking layers. However, at

the top periphery of the worksurface, the more the helix angle is high, the more the fibers inside the top periphery have a low fiber maintaining because the resulting cutting direction moves toward the axial direction as explained in Section 3.2.1. Therefore, increasing the tool helix angle increases the cutting contact stiffness at the bottom edge of the worksurface and decreases the cutting contact stiffness at the top edge of the worksurface.

4. Conclusions

This study involves an experimental investigation to understand the influence of the tool helix angle on the tribo-contact interactions of woven flax fiber reinforced polypropylene composites under milling process. The tribo-contact interaction was studied by analyzing the cutting forces, the frictional performances and the multiscale surface roughness. It can be concluded that:

- The tool helix angle has a significant effect on cutting forces and friction coefficients. Zero helix angle tool induces a brutal engagement in the composite which improve the flax fiber shearing but increases significantly the friction. This can considerably affect the tool wear. Increasing the tool helix angle reduces the shearing efficiency and also the friction due to the progressive engagement of the cutting edge and the uncut fiber extremities on the milled surface which acts as a lubricant.
- The milled surface quality depends on the fibers orientation inside the woven structure of the flax reinforcement. The warp fibers have an efficient shearing during the cutting contact interaction. The weft fibers present different cutting behaviors depending on the contact position between the flax fibers and the cutting edge. This generates important surface roughness in weft fiber zones which is much higher than that of warp fiber zones.
- The milled surface roughness increases by feed increasing. The roughness level induced by down-milling configuration is higher than that of up-milling configuration due to the chip debris that remain on the milled surface. Increasing the tool helix angle increases the uncut fiber extremities which increase the surface roughness but favors the chip clearance from the milled surface which can reduce the roughness level.
- Multiscale surface analysis shows that the pertinent scales to evaluate the helix angle effect are between 50 μm and 1 mm which refers to the flax reinforcement structure scales. The irregularities showed in the weft fiber zones are obvious at the mesoscopic scales.
- Increasing the tool helix angle increases the top fluffing defects and decreases the bottom fluffing defects on the worksurface.

References

[1] Dittenber DB, GangaRao HVS. Critical review of recent publications on use of natural composites in infrastructure. Compos Part A Appl Sci Manuf 2012;43:1419–29. http://dx.doi.org/10.1016/j.compositesa.2011.11.019.

[2] Shalwan A, Yousif BF. In state of art: mechanical and tribological behaviour of polymeric composites based on natural fibres. Mater Des 2013;48:14–24. http://dx.doi.org/10.1016/j.matdes.2012.07.014.

[3] Wambua P, Ivens J, Verpoest I. Natural fibres: can they replace glass in fibre reinforced plastics? Compos Sci Technol 2003;63:1259–64. http://dx.doi.org/10.1016/S0266-3538(03)00096-4.

[4] Faruk O, Bledzki AK, Fink H-P, Sain M. Biocomposites reinforced with natural fibers: 2000–2010. Prog Polym Sci 2012;37:1552–96. http://dx.doi.org/10.1016/j.progpolymsci.2012.04.003.

[5] Pickering KL, Beckermann GW, Alam SN, Foreman NJ. Optimising industrial hemp fibre for composites. Compos Part A Appl Sci Manuf 2007;38:461–8. http://dx.doi.org/10.1016/j.compositesa.2006.02.020.

[6] Durão LMP, Gonçalves DJS, Tavares JMRS, de Albuquerque VHC, Panzera TH, Silva LJ, et al. Drilling delamination outcomes on glass and sisal reinforced plastics. Mater Sci Forum 2012;730–732:301–6. http://dx.doi.org/10.4028/www.scientific.net/MSF.730-732.301.

[7] Naveen PNE, Yasaswi M, Prasad RV. Experimental investigation of drilling parameters on composite materials. J Mech Civ Eng 2012;2:30–7.

[8] Babu GD, Babu KS, Gowd BUM. Effect of machining parameters on milled natural fiber–reinforced plastic composites. J Adv Mech Eng 2013;1:1–12. http://dx.doi.org/10.7726/jame.2013.1001.

[9] Baley C. Analysis of the flax fibres tensile behaviour and analysis of the tensile stiffness increase. Compos – Part A Appl Sci Manuf 2002;33:939–48. http://dx.doi.org/10.1016/S1359-835X(02)00040-4.

[10] Van de Weyenberg I, Ivens J, De Coster A, Kino B, Baetens E, Verpoest I. Influence of processing and chemical treatment of flax fibres on their composites. Compos Sci Technol 2003;63:1241–6. http://dx.doi.org/10.1016/S0266-3538(03)00093-9.

[11] Shah DU. Developing plant fibre composites for structural applications by optimising composite parameters: a critical review. J Mater Sci 2013;48:6083–107 doi:10.1007/s10853-013-7458-7.

[12] Morvan C, Andème-Onzighi C, Girault R, Himmelsbach DS, Driouich A, Akin DE. Building flax fibres: more than one brick in the walls. Plant Physiol Biochem 2003;41:935–44. http://dx.doi.org/10.1016/j.plaphy.2003.07.001.

[13] Chegdani F, Mezghani S, El Mansori M. Experimental study of coated tools effects in dry cutting of natural fiber reinforced plastics. Surf Coatings Technol 2015;284:264–72. http://dx.doi.org/10.1016/j.surfcoat.2015.06.083.

[14] Chegdani F, Mezghani S, El Mansori M, Mkaddem A. Fiber type effect on tribological behavior when cutting natural fiber reinforced plastics. Wear 2015;332–333:772–9. http://dx.doi.org/10.1016/j.wear.2014.12.039.

[15] Mezghani S, Zahouani H, Piezanowski J-J. Multiscale characterizations of painted surface appearance by continuous wavelet transform. J Mater Process Technol 2011;211:205–11. http://dx.doi.org/10.1016/j.jmatprotec.2010.09.011.

[16] Zahouani H, Mezghani S, Vargiolu R, Dursapt M. Identification of manufacturing signature by 2D wavelet decomposition. Wear 2008;264:480–5. http://dx.doi.org/10.1016/j.wear.2006.08.047.

[17] Lee S-H, Zahouani H, Caterini R, Mathia TG. Morphological characterisation of engineered surfaces by wavelet transform. Int J Mach Tools Manuf 1998;38:581–9. http://dx.doi.org/10.1016/S0890-6955(97)00105-3.

[18] Nirmal U, Low KO, Hashim J. On the effect of abrasiveness to process equipment using betelnut and glass fibres reinforced polyester composites. Wear 2012;290–291:32–40. http://dx.doi.org/10.1016/j.wear.2012.05.022.

[19] Li X, Tabil LG, Panigrahi S. Chemical treatments of natural fiber for use in natural fiber-reinforced composites: a review. J Polym Environ 2007;15:25–33. http://dx.doi.org/10.1007/s10924-006-0042-3.

[20] Kalla D, Sheikh-Ahmad J, Twomey J. Prediction of cutting forces in helical end milling fiber reinforced polymers. Int J Mach Tools Manuf 2010;50:882–91. http://dx.doi.org/10.1016/j.ijmachtools.2010.06.005.

[21] Brostow W, Kovacevic V, Vrsaljko D, Whitworth J. Tribology of polymers and polymer-based composites. J Mater Educ 2010;32:273–90.

[22] Myshkin NK, Petrokovets MI, Kovalev AV. Tribology of polymers: adhesion, friction, wear, and mass-transfer. Tribol Int 2005;38:910–21. http://dx.doi.org/10.1016/j.triboint.2005.07.016.

[23] Yousif BF, El-Tayeb NSM. Adhesive wear performance of T-OPRP and UT-OPRP composites. Tribol Lett 2008;32:199–208. http://dx.doi.org/10.1007/s11249-008-9381-7.

[24] Nirmal U, Hashim J, Low KO. Adhesive wear and frictional performance of bamboo fibres reinforced epoxy composite. Tribol Int 2012;47:122–33. http://dx.doi.org/10.1016/j.triboint.2011.10.012.